AAPT PHYSICS EDUCATION | AMERICAN JOURNAL of PHYSICS

# Empirical exploration of timelike geodesics around a rotating wormhole

Thomas Müller and Oliver Fechtig

Citation: American Journal of Physics **84**, 375 (2016); doi: 10.1119/1.4943250
View online: http://dx.doi.org/10.1119/1.4943250
View Table of Contents: http://scitation.aip.org/content/aapt/journal/ajp/84/5?ver=pdfcov
Published by the American Association of Physics Teachers



# Empirical exploration of timelike geodesics around a rotating wormhole

Thomas Müller[a)]
*Visualization Research Center, University of Stuttgart, Allmandring 19, 70569 Stuttgart, Germany*

Oliver Fechtig[b)]
*Fanny-Leicht Gymnasium Stuttgart, Fanny-Leicht Str. 13, 70563 Stuttgart-Vaihingen, Germany*

(Received 15 August 2015; accepted 17 February 2016)

In an advanced course on general relativity, some exotic spacetimes like wormholes with a more complex topology than the standard Schwarzschild spacetime can be studied in detail. In this regard, it has been pointed out by Morris and Thorne that wormholes could be a valuable tool for teaching general relativity. In this paper, we claim rotating wormholes might also have a pedagogical role in general relativity, and present an empirical approach to explore periodic orbits of such, that could be applied also to other spacetimes. © *2016 American Association of Physics Teachers.*
[http://dx.doi.org/10.1119/1.4943250]

## I. INTRODUCTION

The paper by Morris and Thorne in 1988 showed that wormholes can be a valuable tool for teaching general relativity.[1] Certainly, due to science fiction movies such as *Contact* (1997) and *Interstellar* (2014),[4] interest in these exotic spacetimes (in physics and astronomy courses) has vastly increased. Hence, in addition to black holes, wormholes have become good motivators for teaching geodesics within general relativity, which is a standard topic aimed to get a deeper understanding of the structure of a spacetime.

The simplicity of the Ellis wormhole[2] metric, which has nevertheless an interesting topology, makes it straightforward to visualize the inner geometry of the spacetime.[3] It does so by embedding a two-dimensional hypersurface into the Euclidean geometry, in order to study the qualitative behavior of geodesics by means of the Euler-Lagrangian[5] formalism. With this in mind, we generalize this investigation by adding rotation to the wormhole spacetime because, as a practical matter, nearly everything in space has rotation. Also, from the educational point of view, we find that several new features arise that are not present in the non-rotating Ellis wormhole. Here, we use the rotating wormhole spacetime by Teo[6] and restrict the gravitational potentials to a minimum so that we can focus on the influence of the spinning of the wormhole onto lightlike and timelike geodesics.

The geodesics in the Ellis wormhole spacetime have a very simple structure. While they appear quite similar to those in the Schwarzschild spacetime at first glance, the main difference is that timelike and lightlike geodesics all follow the same trajectory as long as they start from the same point and head in the same direction. Even the initial velocity of a timelike geodesic has no influence on its trajectory. A detailed discussion of the geodesics in the Ellis spacetime can be found in Ref. 7. In the rotating wormhole spacetime, this changes significantly, leading to interesting geodesics around the wormhole throat.

The main focus of this paper is to show that bound timelike orbits, and in particular, periodic orbits, exist in the rotating wormhole spacetime. To find them, we follow a half-theoretical, half-empirical approach. For this, we first use the Euler-Lagrangian formalism and the geodesic equation to discuss the qualitative behavior of geodesics. Then, by exploiting the orbital equation and the constants of motion, we empirically study bound timelike geodesics if they are periodic and what shape they have.

A discussion about periodic orbits and their taxonomy in Schwarzschild spacetime is given by Levin and Perez-Giz.[8] These authors also present an in-depth investigation about timelike orbits around spinning black holes.[9] An analytic solution to bound orbits in Kerr spacetime is discussed by Fujita and Hikida.[10] There are also numerous publications about the special case of circular orbits in different spacetimes.[11–14] Details of wormhole physics can be found in the book by Visser.[15] For our discussion here, we make use of the GeodesicViewer,[16,17] which can interactively visualize geodesics in different 2D and 3D representations. This program is based on the Motion4D library[18] and can thus be used to explore geodesics in a multitude of spacetimes.

The structure of this paper is as follows. In Sec. II, we introduce the Teo metric and our restrictions to a particular set of gravitational potentials. We also deduce the reference frame of a locally non-rotating observer and the embedding diagram. In Sec. III, we give a qualitative discussion of lightlike and timelike geodesics in the restricted Teo metric by means of the Euler-Lagrangian formalism. The main focus, however, is on bound timelike orbits and how periodic orbits could be found even without an analytic solution to the geodesic equation, as we will discuss in Sec. IV.

## II. TEO METRIC

We start with the axisymmetric, rotating, stationary spacetime metric given by Teo.[6] In spherical coordinates, $t \in (-\infty, \infty)$, $r \in [r_0, \infty)$, $\vartheta \in (0, \pi)$, $\varphi \in [0, 2\pi)$, the line element reads

$$\mathrm{d}s^2 = -N^2c^2\mathrm{d}t^2 + \frac{r}{r-b}\mathrm{d}r^2 + r^2K^2\left[\mathrm{d}\vartheta^2 + \sin^2\vartheta\left(\mathrm{d}\varphi - \frac{\omega}{c}c\,\mathrm{d}t\right)^2\right], \tag{1}$$

where the gravitational potentials $N$, $K$, $b$, and $\omega$ all depend on $r$ and $\vartheta$. However, for educational purposes, we restrict the gravitational potentials such that we can put our focus on the rotation of the wormhole spacetime.

### A. Specialized metric

For the rest of this article, we restrict the potentials to

$$b(r)=\frac{b_0^2}{r},\quad K(r)=N(r)\equiv 1,\quad \text{and}\quad \omega(r)=\frac{cb_0^2}{2r^3},\tag{2}$$

where Appendix A gives a brief motivation for how we came to this choice. Please note that the parameter $b_0$ defines the shape of the wormhole throat as well as its rotation. In the limit $b_0\to 0$, we end up with the static Minkowski spacetime in spherical coordinates.

Transforming to the proper radial coordinate $l^2=r^2-b_0^2$, the general Teo metric (1) simplifies to

$$\begin{aligned}\mathrm{d}s^2=&-c^2\mathrm{d}t^2+\mathrm{d}l^2+\left(l^2+b_0^2\right)\\&\times\left\{\mathrm{d}\vartheta^2+\sin^2\vartheta\left[\mathrm{d}\varphi-\frac{b_0^2}{2\left(l^2+b_0^2\right)^{3/2}}c\,\mathrm{d}t\right]^2\right\},\end{aligned}\tag{3}$$

with metric $\mathbf{g}=g_{\mu\nu}\mathrm{d}x^\mu\mathrm{d}x^\nu$ and with coefficients

$$g_{tt}=-c^2+\frac{b_0^4c^2\sin^2\vartheta}{4\left(l^2+b_0^2\right)^2},\quad g_{ll}=1,\tag{4a}$$

$$g_{\vartheta\vartheta}=l^2+b_0^2,\quad g_{t\varphi}=g_{\varphi t}=-\frac{1}{2}\frac{b_0^2c\sin^2\vartheta}{\sqrt{l^2+b_0^2}},\tag{4b}$$

and

$$g_{\varphi\varphi}=\left(l^2+b_0^2\right)\sin^2\vartheta.\tag{4c}$$

The resulting Christoffel symbols read

$$\Gamma^l_{tt}=\frac{b_0^4c^2l\sin^2\vartheta}{2\left(l^2+b_0^2\right)^3},\quad \Gamma^\vartheta_{tt}=-\frac{b_0^4c^2\sin\vartheta\cos\vartheta}{4\left(l^2+b_0^2\right)^3},\tag{5a}$$

$$\Gamma^t_{tl}=\frac{3b_0^4l\sin^2\vartheta}{8\left(l^2+b_0^2\right)^3},\quad \Gamma^\varphi_{t\vartheta}=-\frac{b_0^2c\cot\vartheta}{2\left(l^2+b_0^2\right)^{3/2}},\tag{5b}$$

$$\Gamma^l_{t\varphi}=-\frac{b_0^2cl\sin^2\vartheta}{4\left(l^2+b_0^2\right)^{3/2}},\quad \Gamma^l_{\varphi\varphi}=-l\sin^2\vartheta,\tag{5c}$$

$$\Gamma^\vartheta_{t\varphi}=\frac{b_0^2c\sin\vartheta\cos\vartheta}{2\left(l^2+b_0^2\right)^{3/2}},\quad \Gamma^\vartheta_{l\vartheta}=\frac{l}{l^2+b_0^2},\tag{5d}$$

$$\Gamma^t_{l\varphi}=-\frac{3b_0^2l\sin^2\vartheta}{4c\left(l^2+b_0^2\right)^{3/2}},\quad \Gamma^l_{\vartheta\vartheta}=-l,\tag{5e}$$

$$\Gamma^\varphi_{\vartheta\varphi}=\cot\vartheta,\quad \Gamma^\vartheta_{\varphi\varphi}=-\sin\vartheta\cos\vartheta,\tag{5f}$$

$$\Gamma^\varphi_{tl}=\frac{b_0^2cl\left[3b_0^4\sin^2\vartheta+4\left(l^2+b_0^2\right)^2\right]}{16\left(l^2+b_0^2\right)^{9/2}},\tag{5g}$$

and

$$\Gamma^\varphi_{l\varphi}=-\frac{l\left[3b_0^4\sin^2\vartheta-8\left(l^2+b_0^2\right)^2\right]}{8\left(l^2+b_0^2\right)^3}.\tag{5h}$$

To find the trajectories of geodesics, we could now integrate the geodesic equation

$$\frac{\mathrm{d}^2x^\mu}{\mathrm{d}\lambda^2}+\Gamma^\mu_{\nu\sigma}\frac{\mathrm{d}x^\nu}{\mathrm{d}\lambda}\frac{\mathrm{d}x^\sigma}{\mathrm{d}\lambda}=0,\tag{6}$$

where $\lambda$ is an affine parameter. Because Eq. (6) is a second-order ordinary differential equation, we need not only an initial position but also an initial direction. The latter shall be defined with respect to a local reference frame that is given by a local tetrad.

### B. Local tetrad

In a stationary axisymmetric spacetime, two natural local tetrads could be defined: a tetrad that is static with respect to the asymptotic background, and a tetrad that is locally non-rotating; see Misner *et al.*[19] for a detailed discussion about locally non-rotating frames (LNRF). The ansatz for the LNRF case reads

$$\begin{aligned}&\mathbf{e}_{(l)}=\partial_l,\quad \mathbf{e}_{(\vartheta)}=\frac{1}{\sqrt{l^2+b_0^2}}\partial_\vartheta,\\&\mathbf{e}_{(t)}=A\partial_t+B\partial_\varphi,\quad \text{and}\quad \mathbf{e}_{(\varphi)}=C\partial_\varphi,\end{aligned}\tag{7}$$

and with the orthonormality condition $\langle\mathbf{e}_{(i)},\mathbf{e}_{(j)}\rangle=\eta_{(i)(j)}$, where $\eta=(i)(j)=\mathrm{diag}(-1,1,1,1)$ represents the Minkowski metric, and $\langle\,,\rangle$ the scalar product with respect to the metric $\mathbf{g}$, we then have

$$\begin{aligned}&\mathbf{e}_{(t)}=\frac{1}{c}\partial_t+\frac{b_0^2}{2\left(l^2+b_0^2\right)^{3/2}}\partial_\varphi,\quad \mathbf{e}_{(l)}=\partial_l,\\&\mathbf{e}_{(\vartheta)}=\frac{1}{\sqrt{l^2+b_0^2}}\partial_\vartheta,\quad \text{and}\quad \mathbf{e}_{(\varphi)}=\frac{1}{\sin\vartheta\sqrt{l^2+b_0^2}}\partial_\varphi.\end{aligned}\tag{8}$$

For $b_0=0$, we obtain the static tetrad of the Minkowski spacetime in spherical coordinates. With respect to this frame, the stress-energy tensor immediately shows that we would need exotic matter to maintain this wormhole geometry (see Appendix B).

### C. Embedding diagram

The inner geometry of a spacetime can be partially visualized by embedding a two-dimensional hypersurface into the three-dimensional Euclidean space that can be described by the line element

$$\mathrm{d}\sigma^2_{\mathrm{eucl}}=\left[1+\left(\frac{\mathrm{d}z}{\mathrm{d}r}\right)^2\right]\mathrm{d}r^2+r^2\mathrm{d}\varphi^2.\tag{9}$$

Comparing this line element with the hypersurface $(t=\text{const},\ \vartheta=\pi/2)$ of the Teo metric in Eq. (3), where $r=\sqrt{l^2+b_0^2}\in[b_0,\infty)$, we obtain a differential equation for $z$ with respect to $r$ that can be directly integrated. The resulting shape function $z(r)$ reads

$$z(r)=\pm b_0\ln\left(\frac{\sqrt{r^2-b_0^2}+r}{b_0}\right),\tag{10}$$

where $(+)$ represents the upper and $(-)$ the lower universe. Figure 1 shows the embedding diagram for the shape function, guided by Eq. (10), which is equivalent to the static Ellis wormhole shape function with the same throat parameter $b_0$. The circles represent points of constant radial coordinate $l$, whereas the lines perpendicular to the circles are the coordinate lines for constant $\varphi$. The rotation of the spacetime is not shown in this diagram.

## III. GEODESICS

In the following, we focus on geodesics in the $(\vartheta = \pi/2)$ hypersurface and use the Euler-Lagrangian formalism to study their behavior. Expressing the derivative of a coordinate with respect to the affine parameter $\lambda$ by a dot (as in $\dot{t} = \mathrm{d}t/\mathrm{d}\lambda$), the Lagrangian function $\mathcal{L}$ reads

$$\mathcal{L} = -c^2\dot{t}^2 + \dot{l}^2 + \left(l^2 + b_0^2\right)\left[\dot{\varphi} - \frac{b_0^2}{2\left(l^2 + b_0^2\right)^{3/2}}c\dot{t}\right]^2. \tag{11}$$

From the Euler-Lagrangian equations

$$\frac{\mathrm{d}}{\mathrm{d}\lambda}\frac{\partial\mathcal{L}}{\partial\dot{x}^\mu} - \frac{\partial\mathcal{L}}{\partial x^\mu} = 0, \quad \mu = \{t, l, \varphi\}, \tag{12}$$

we obtain two constants of motion

$$c_1 = 2c^2\dot{t} + \frac{b_0^2 c}{\sqrt{l^2 + b_0^2}}\left[\dot{\varphi} - \frac{b_0^2}{2\left(l^2 + b_0^2\right)^{3/2}}c\dot{t}\right], \tag{13a}$$

and

$$c_2 = \left(l^2 + b_0^2\right)\left[\dot{\varphi} - \frac{b_0^2}{2\left(l^2 + b_0^2\right)^{3/2}}c\dot{t}\right]. \tag{13b}$$

These constants can be solved for the coordinate derivatives

$$\dot{t} = \frac{c_1}{2c^2} - \frac{b_0^2 c_2}{2c\left(l^2 + b_0^2\right)^{3/2}}, \tag{14a}$$

and

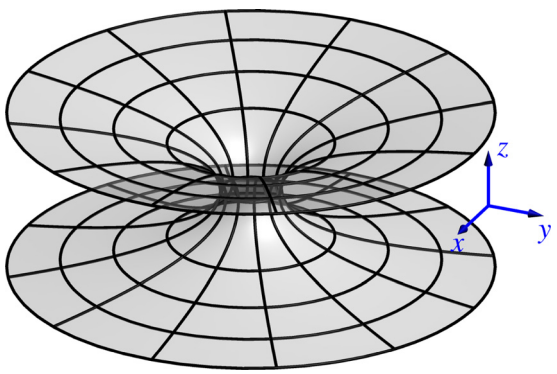


Fig. 1. Embedding diagram of the $(t = \text{const}, \vartheta = \pi/2)$ hypersurface for $b_0 = 1$ and $r_{\max} = 8$. The bottleneck represents the wormhole throat. Note, only the surface is part of the spacetime.

$$\dot{\varphi} = \frac{c_2}{l^2 + b_0^2} + \frac{b_0^2 c_1}{4c\left(l^2 + b_0^2\right)^{3/2}} - \frac{b_0^4 c_2}{4\left(l^2 + b_0^2\right)^3}. \tag{14b}$$

The remaining differential equation for the proper radial coordinate $l$ can be deduced from the Lagrangian (11) together with the constants of motion

$$\dot{l}^2 = \kappa c^2 + c^2\left[\frac{c_1}{2c^2} - \frac{b_0^2 c_2}{2c\left(l^2 + b_0^2\right)^{3/2}}\right]^2 - \frac{c_2^2}{l^2 + b_0^2}, \tag{15}$$

where $\kappa = 0$ for lightlike and $\kappa = -1$ for timelike geodesics.

### A. Lightlike geodesics

As the geodesic equation (6) is a second-order ordinary differential equation, we need not only an initial position but also an initial direction. The initial position is given by the observer's location $(t = t_{\text{obs}}, l = l_{\text{obs}}, \vartheta = \pi/2, \varphi = 0)$, while the initial direction is defined with respect to its local reference frame, given in Eq. (8). As we consider only geodesics in the $(\vartheta = \pi/2)$ hypersurface, we only need the initial angle $\xi$. Hence,

$$\mathbf{y} = \pm\mathbf{e}_{(t)} + \cos\xi\,\mathbf{e}_{(l)} + \sin\xi\,\mathbf{e}_{(\varphi)}, \tag{16}$$

where $(+)$ represents a future-directed and $(-)$ a past-directed light ray. Replacing the tetrad vectors by their coordinate representations $\mathbf{e}_{(i)} = e^\mu_{(i)}\partial_\mu$, we immediately obtain the components $y^\mu = (\dot{t}, \dot{l}, 0, \dot{\varphi})_{\dot{\lambda}=0} = (\dot{t}_{\text{obs}}, \dot{l}_{\text{obs}}, 0, \dot{\varphi}_{\text{obs}})$ of the initial direction $\mathbf{y} = y^\mu\partial_\mu = \dot{t}_{\text{obs}}\partial_t + \dot{l}_{\text{obs}}\partial_l + \dot{\varphi}_{\text{obs}}\partial_\varphi$; thus,

$$\dot{t}_{\text{obs}} = \pm\frac{1}{c}, \quad \dot{l}_{\text{obs}} = \cos\xi \tag{17a}$$

and

$$\dot{\varphi}_{\text{obs}} = \pm\frac{b_0^2}{2\left(l_{\text{obs}}^2 + b_0^2\right)^{3/2}} + \frac{\sin\xi}{\sqrt{l_{\text{obs}}^2 + b_0^2}}. \tag{17b}$$

Substituting Eq. (17) into Eq. (13) yields

$$c_1 = 2c + \frac{b_0^2 c\sin\xi}{l_{\text{obs}}^2 + b_0^2}, \quad \text{and} \quad c_2 = \sqrt{l_{\text{obs}}^2 + b_0^2}\sin\xi \tag{18}$$

for the constants of motion.

#### 1. Lightlike circular orbits

A particular solution of the geodesic equation, which we already know from the Ellis spacetime, is the circular orbit (see Ref. 7). For that, the initial angle has to be $\xi = \pm\pi/2$, and the derivative of the proper radial coordinate has to vanish identically $(\dot{l} \equiv 0)$. From Eq. (15) with $\kappa = 0$, we see that for $\xi = \pm\pi/2$ a light ray always starts with vanishing $\dot{l}$, but we cannot conclude that it will vanish identically. Otherwise, there would be an infinite number of lightlike circular orbits.

Hence, we need the geodesic equation (6), which yields

$$\frac{\mathrm{d}^2 l}{\mathrm{d}\lambda^2} + \Gamma^l_{tt}\left(\frac{\mathrm{d}t}{\mathrm{d}\lambda}\right)^2 + 2\Gamma^l_{t\varphi}\frac{\mathrm{d}t}{\mathrm{d}\lambda}\frac{\mathrm{d}\varphi}{\mathrm{d}\lambda} + \Gamma^l_{\varphi\varphi}\left(\frac{\mathrm{d}\varphi}{\mathrm{d}\lambda}\right)^2 = 0. \tag{19}$$

Note that Eq. (19) is also valid for timelike geodesics. Inserting Eqs. (14a) and (14b) into Eq. (19), using the

constants of motion [see Eq. (18)] for prograde motion ($\xi = +\pi/2$), and letting $l_{\rm obs} = l$ yields

$$\frac{\mathrm{d}^2 l}{\mathrm{d}\lambda^2} - \frac{l\left(2l^2 + 5b_0^2\right)}{2\left(l^2 + b_0^2\right)^2} = 0. \tag{20}$$

Hence, in the prograde case there exists a lightlike circular orbit only for $l_{\rm co} = 0$. In the retrograde case, where $\xi = -\pi/2$, we obtain

$$\frac{\mathrm{d}^2 l}{\mathrm{d}\lambda^2} - \frac{l\left(2l^2 - b_0^2\right)}{2\left(l^2 + b_0^2\right)^2} = 0. \tag{21}$$

Thus, we have three retrograde lightlike circular orbits at $l_{\rm co} = 0$ and $l_{\rm rco\pm} = \pm b_0/\sqrt{2}$.

### 2. The apparent size of the wormhole

The apparent size of the Ellis wormhole is defined by all initial directions where the corresponding light rays approach the wormhole throat only asymptotically while still staying at the same side. In the case of the Schwarzschild black hole, the apparent size equals the shadow of the black hole, which is defined by the geodesics approaching the photon orbit asymptotically.

For our simplified Teo wormhole spacetime, we define its apparent size by the initial direction $\xi_p$, which approaches the wormhole throat asymptotically in a prograde sense, and by the initial direction $\xi_r$, which approaches the circular orbit $l_{\rm rco+}$ asymptotically in a retrograde sense (see Fig. 2). Thereby, we restrict the apparent size to the equatorial plane because all the other directions are much more difficult to find.

Here, we also have to take into account that we have to trace light rays back in time, which means we must use the minus sign in Eq. (17). If we insert the constants of motion into Eq. (15) and let $\dot{l} = 0$ and $l = 0$ for the prograde orbit, we obtain the observation angle

$$\xi_p = \pi - \arcsin\frac{-2\left(x_{\rm obs}^2 + 1\right)}{3\left(x_{\rm obs}^2 + 1\right)^{3/2} + 1}, \tag{22}$$

where we have used the scaled coordinate $x_{\rm obs} = l_{\rm obs}/b_0$.

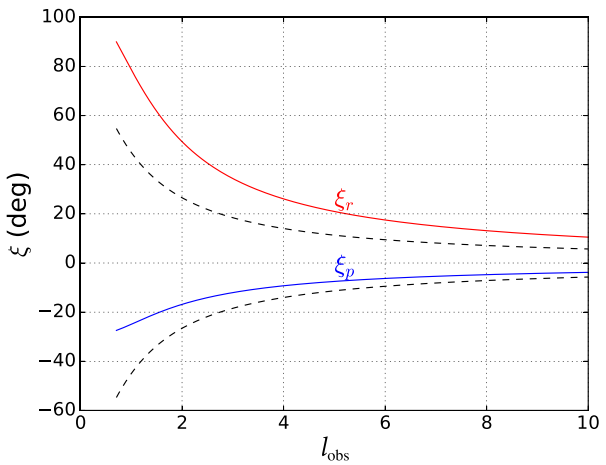


Fig. 2. The apparent angular size $\Delta\xi = |\xi_p - \xi_r|$ of the rotating Teo wormhole in the equatorial plane is defined by the critical angles $\xi_p$ and $\xi_r$. The observer located at $l = l_{\rm obs}$ looks towards the wormhole ($\xi = 0$) and the throat parameter reads $b_0 = 1$. The dashed lines represent the apparent size of an Ellis wormhole.

On the other hand, the retrograde case, where $\dot{l} = 0$ and $l = b_0/\sqrt{2}$, the observation angle is given by

$$\xi_r = \pi - \arcsin\frac{2\left(x_{\rm obs}^2 + 1\right)}{2(2/3)^{3/2}\left(x_{\rm obs}^2 + 1\right)^{3/2} + 1}. \tag{23}$$

Both angles are valid for $l_{\rm obs} \geq b_0/\sqrt{2}$.

For comparison only, the limiting angle $\xi$ for an Ellis wormhole is given by $\xi = \pi - \arcsin(1/\sqrt{x_{\rm obs}^2 + 1})$. It is immediately clear from Fig. 2 that the rotating wormhole shows an asymmetry regarding its apparent size.

## B. Timelike geodesics

The initial position for a timelike geodesic is also given by the observer's location $(t = t_{\rm obs}, l = l_{\rm obs}, \vartheta = \pi/2, \varphi = 0)$. However, the initial direction follows from the four-velocity:

$$\mathbf{u} = c\gamma(\mathbf{e}_{(t)} + \beta\cos\xi\,\mathbf{e}_{(l)} + \beta\sin\xi\,\mathbf{e}_{(\varphi)}), \tag{24}$$

which itself is defined by the three-velocity $v$ with respect to the observer's local reference frame. Furthermore, we have $\mathbf{u}^2 = -c^2$, $\xi \in [0, 2\pi]$, $0 \leq \beta = v/c < 1$, and $\gamma = 1/\sqrt{1-\beta^2}$. Here, we concentrate only on future-directed geodesics. Then, the constants of motion [see Eq. (13)] can be expressed in the following way:

$$c_1 = c^2\gamma\left(2 + \frac{b_0^2\beta\sin\xi}{l_{\rm obs}^2 + b_0^2}\right), \tag{25a}$$

and

$$c_2 = c\gamma\beta\sqrt{l_{\rm obs}^2 + b_0^2}\sin\xi. \tag{25b}$$

In the special case where the initial velocity vanishes ($\beta = 0$), the constants of motion reduce to $c_1 = 2c^2$ and $c_2 = 0$, and we obtain

$$\dot{t}_0 = 1, \quad \dot{\varphi}_0 = \frac{b_0^2 c}{2\left(l_{\rm obs}^2 + b_0^2\right)^{3/2}}, \quad \text{and} \quad \dot{l}_0^2 = 0. \tag{26}$$

Inserting all these into the geodesic equation for the coordinate $l$, using Eq. (19), yields $\mathrm{d}^2 l/\mathrm{d}\tau^2 \equiv 0$, where we have replaced the affine parameter $\lambda$ by the proper time $\tau$. Thus, any massive particle with zero initial velocity follows a circular orbit around the simplified Teo wormhole. Because of the relation $\dot{t} = \mathrm{d}t/\mathrm{d}\tau = 1$, coordinate time and proper time are the same on these orbits. The orbital period $\tau_{2\pi} = 2\pi/\omega$ with the angular velocity $\omega = \dot{\varphi}$ is given by

$$\tau_{2\pi} = \frac{4\pi\left(l^2 + b_0^2\right)^{3/2}}{b_0^2 c}, \tag{27}$$

with a minimum at $l = 0$.

## IV. BOUND TIMELIKE ORBITS

If we tinker a little bit with Eq. (15) for timelike geodesics, we see that there exist bound orbits around the wormhole throat. Without loss of generality, we assume that the starting position $l = l_{\rm obs}$, is a turning point of the bound orbit. Thus

$$\dot{l}^2|_{l=l_{\rm obs}} = c^2\gamma^2\beta^2\cos^2\xi = 0, \tag{28}$$

meaning that either $\beta = 0$ or $\xi = \pm\pi/2$. The special case $\beta = 0$ was already discussed in Sec. III B. Here, we fix $\xi = \pi/2$, which places $\beta$ in the range $(-1, 1)$.

To be a turning point for a bound orbit, where $l < l_{\rm obs}$ in a small neighborhood, the second derivative $\mathrm{d}^2l/\mathrm{d}\tau^2$ at the position $l = l_{\rm obs}$ has to be negative. From Eq. (19) for the proper radial coordinate $l$, the coordinate derivatives of Eq. (14), and the constants of motion in Eq. (25), the second derivative of $l$ with respect to proper time $\tau$ evaluated at $l = l_{\rm obs}$ becomes

$$\left.\frac{\mathrm{d}^2l}{\mathrm{d}\tau^2}\right|_{l=l_{\rm obs}} = \frac{c^2\beta\gamma^2 l_{\rm obs}\left[2\beta\left(l_{\rm obs}^2 + b_0^2\right) + 3b_0^2\right]}{2\left(l_{\rm obs}^2 + b_0^2\right)^2}. \tag{29}$$

As long as $l_{\rm obs} > 0$, it must be true that

$$\beta[2\beta(l_{\rm obs}^2 + b_0^2) + 3b_0^2] < 0, \tag{30}$$

as shown in Fig. 3. Hence, $\beta$ cannot be positive. If $\mathrm{d}^2l/\mathrm{d}\tau^2 = 0$, we obtain circular orbits, where

$$\beta = -\frac{3}{2}\frac{b_0^2}{l_{\rm obs}^2 + b_0^2}. \tag{31}$$

Because $\beta$ is bounded by $-1$ from below, retrograde circular orbits with $\beta \neq 0$ exist only for $l_{\rm obs}^2 > b_0^2/2$. If Eq. (30) is not fulfilled, i.e., $\mathrm{d}^2l/\mathrm{d}\tau^2 > 0$, we still have $\dot{l}|_{l=l_{\rm obs}} = 0$, and thus the geodesic passes its point of closest approach to the wormhole throat.

### A. Periodic orbits

So far, we know whether a timelike trajectory is a bound orbit or not. But, we also would like to know if the bound orbit is periodic. As we do not have an analytic solution to the geodesic equation, we have to find periodic orbits in a more empirical way. For that, we derive a subset of the orbital equation $l = l(\varphi)$ from Eqs. (15) and (14b). With $\mathrm{d}l/\mathrm{d}\varphi = \dot{l}/\dot{\varphi}$, we obtain

$$\frac{\mathrm{d}l}{\mathrm{d}\varphi} = \frac{\pm\sqrt{-c^2 + c^2\left(\frac{c_1}{2c^2} - \frac{b_0^2c_2}{2c\left(l^2+b_0^2\right)^{3/2}}\right)^2 - \frac{c_2^2}{l^2+b_0^2}}}{\frac{c_2}{l^2+b_0^2} + \frac{b_0^2c_1}{4c\left(l^2+b_0^2\right)^{3/2}} - \frac{b_0^4c_2}{4\left(l^2+b_0^2\right)^3}} \equiv \rho(b_0, l_{\rm obs}, l), \tag{32}$$

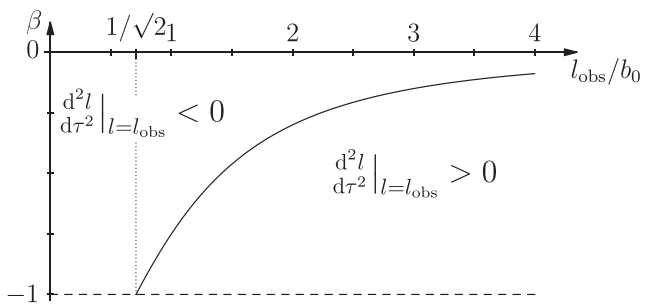


Fig. 3. Depending on the initial position $l_{\rm obs}$ and the initial velocity $\beta$, the timelike geodesic is either a bound orbit, $\mathrm{d}^2l/\mathrm{d}\tau^2 < 0$, a circular orbit, $\mathrm{d}^2l/\mathrm{d}\tau^2 = 0$ (solid line), or a geodesic that passes its point of closest approach.

with separation of variables yielding

$$\int_{\varphi'=0}^{\varphi}\mathrm{d}\varphi' = \int_{l=l_{\rm obs}}^{L}\frac{\mathrm{d}l}{\rho(b_0, l_{\rm obs}, l)}. \tag{33}$$

While the left-hand side can be evaluated immediately, the upper bound of the right-hand integral is not yet clear. To be a periodic orbit, $L$ should be $l_{\rm obs}$, but this does not make any sense.

A closer look on Eq. (15) shows that $\dot{l}^2$ is symmetric with respect to $l$ with maximum at $l = 0$. A little more effort is needed to show that $\dot{l}^2$ is also strongly monotonic. Thus, any bound orbit is symmetric in $l$ and must traverse the wormhole throat. Hence, $L = 0$ and we have

$$\varphi = \int_{l_{\rm obs}}^{0}\frac{\mathrm{d}l}{\rho(b_0, l_{\rm obs}, l)}. \tag{34}$$

But, of course, Eq. (34) covers only a portion of the trajectory. Figure 4 shows the $\bar{\varphi}$–$\beta$ plot of Eq. (34) for $b_0 = 1$ and $l_{\rm obs} = 1$, where $\bar{\varphi} = \varphi/2\pi$. Now, if $\bar{\varphi}$ is a *rational* number—i.e., $\bar{\varphi} = n/m$, with $n, m$ being integers—then we have a periodic orbit.

The resolution of Fig. 4 is too low to read the values from the printed graph. Thus, the data values should be read into a plotting tool[20] (or any drawing tool where zooming is possible), so for a given rational $\bar{\varphi}$, the corresponding approximate value $\beta$ can be determined.

### B. The azimuth angle $\varphi$

Some more information about the shape of the bounded orbits can be extracted from the differential equation for the azimuth angle $\varphi$. Here, we show that $\varphi$ is not a monotonic function, which means that $\dot{\varphi}$ changes sign.

With the substitution $z = \sqrt{l^2/b_0^2 + 1}$, Eq. (14b) can be written as

$$\dot{\varphi} = \frac{1}{b_0^6 z^6}\left(c_2b_0^4z^4 + \frac{b_0^5c_1}{4c}z^3 - \frac{b_0^4c_2}{4}\right). \tag{35}$$

The condition $\dot{\varphi} = 0$ together with the constants of motion delivers the quartic equation

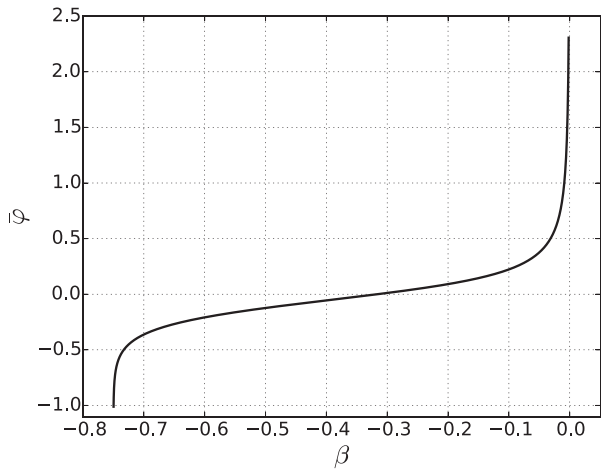


Fig. 4. Equation (34) is plotted as a function of $\beta$ for $b_0 = 1$ and $l_{\rm obs} = 1$ ($\bar{\varphi} = \varphi/2\pi$). To be a bound orbit, the velocity $\beta$ has to be in the domain $[-0.75, 0)$.

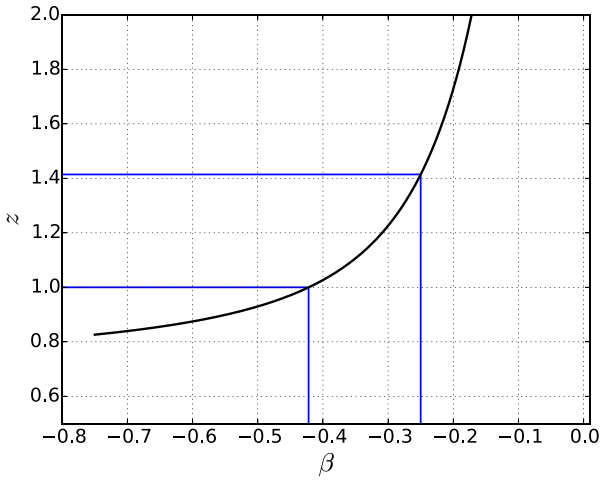


Fig. 5. The roots $z$ of the quartic in Eq. (36) depending on the velocity $\beta$ for $b_0 = 1$ and $l_{\text{obs}} = 1$ ($z_{\text{obs}} = \sqrt{2}$).

$$q(z) = z^4 + az^3 - \frac{1}{4} = 0, \quad \text{with} \quad a = \frac{2z_{\text{obs}}^2 + \beta}{4\beta z_{\text{obs}}^3}, \tag{36}$$

which is of interest only in the domain $z \in [1, z_{\text{obs}}]$. In principle, this quartic equation could be solved analytically. But here, we will first discuss its qualitative behavior and will then solve it numerically.

The extrema of the quartic in Eq. (36) are given by $z_0 = 0$ and $z_1 = -3a/4$. The second derivative of $q$ shows that $z_0$ is an indefinite point and $z_1$ is a minimum. Furthermore, $q(z_0) < 0$, $q(z_1) = -27a^4/256 - 1/4 < 0$, and $\lim_{z\to\infty} q(z) \to \infty$. Thus, there is always a root in the domain $[z_1, \infty)$ that can be found numerically. Figure 5 shows the roots $z$ of Eq. (36) for $b_0 = 1$ and $l_{\text{obs}} = 1$ depending on the velocity $\beta$. As $z$ is limited by $[1, z_{\text{obs}} = \sqrt{2}]$, $\dot{\varphi}$ changes sign only for velocities $\beta$ in the domain $(-0.422, -0.25)$. (See Figs. 8 and 9 for two examples showing a change in direction regarding $\varphi$.)

### C. Examples

With the currently discussed method at hand, we can now search for periodic orbits within the simplified Teo wormhole spacetime. For the following figures, the spherical

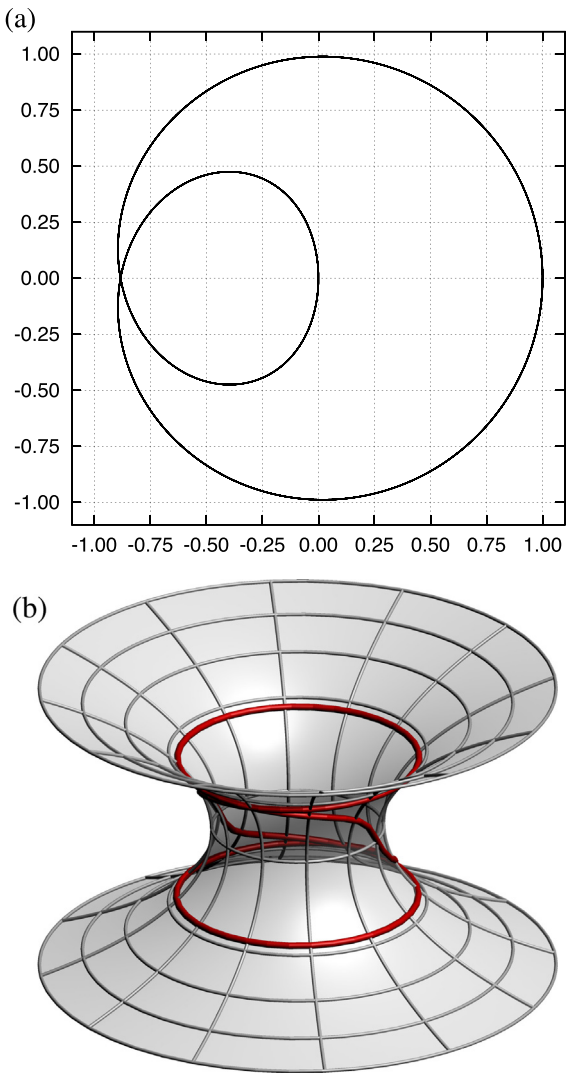


Fig. 6. (a) $xy$-plot and (b) embedding diagram for $\bar{\varphi} = -3/4$ and $\beta = -0.747802$.

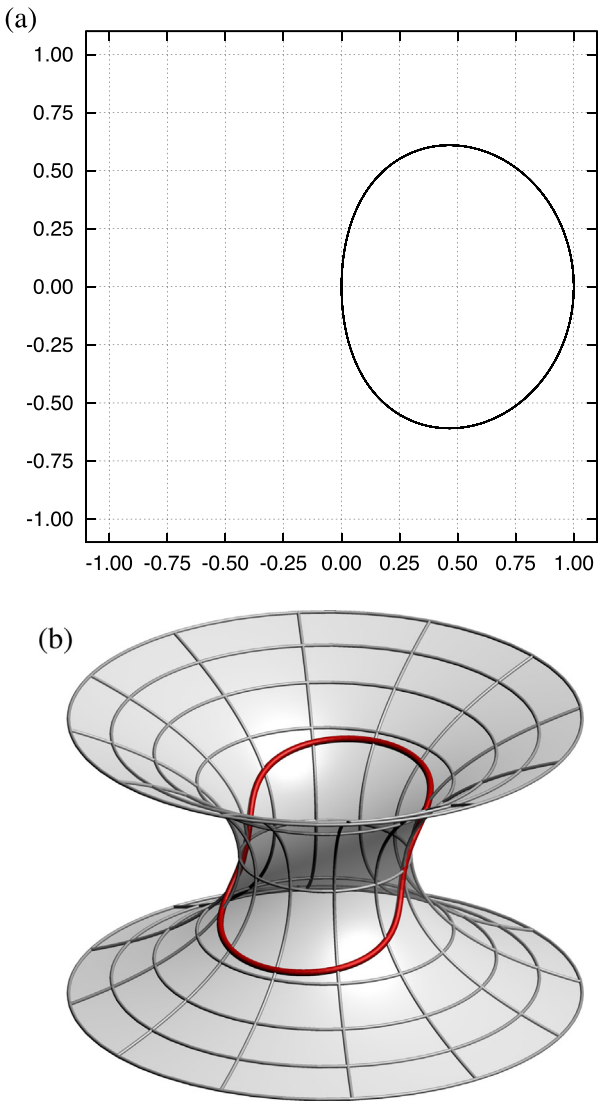


Fig. 7. (a) $xy$-plot and (b) embedding diagram for $\bar{\varphi} = -1/4$ and $\beta = -0.636774$.

coordinates $(l, \varphi)$ are mapped to Cartesian coordinates by means of

$$x = l\cos\varphi \quad \text{and} \quad y = l\sin\varphi. \tag{37}$$

Because $l$ can also be negative, the corresponding trajectories shown in an embedding diagram can deviate from the shapes shown in the $xy$-plot.

Figure 6 shows the periodic orbit for $\bar{\varphi} = -3/4$, where $\beta = -0.747802$. As $\varphi = 2\pi\bar{\varphi}$ gives only the way from $l_{\text{obs}}$ to $l = 0$, we see that after $\varphi = -3\pi/2$ we have only finished one-fourth of the orbit. Hence, a full revolution is achieved for $\varphi = -6\pi$. This becomes even more clear when showing the trajectory in the embedding diagram where it becomes clear that the trajectory has to orbit the wormhole throat three times to close. Figure 7 shows the periodic orbit for $\bar{\varphi} = -1/4$, where $\beta = -0.636774$. Here, we need $\varphi = -2\pi$ to complete the orbit. Figure 8 shows the extreme case where $\bar{\varphi} = 0$. This is the exclusive periodic orbit that does not travel around the wormhole throat. Hence, $\varphi = 0$ again when the orbit is finished. However, this becomes obvious only in the embedding diagram representation. With $\beta = -0.316205$, we can also read from Fig. 5 that the orbit is in the range where $\dot{\varphi}$ changes sign. This happens at $l = \pm 0.6289$.

Figure 9 shows the periodic orbit for $\bar{\varphi} = 1/28$, where $\beta = -0.266165$. The orbit is closed after $\varphi = 2\pi$ and $\dot{\varphi}$ changes sign multiple times at $l = \pm 0.8966$.

Figure 4 shows an example that even though the initial velocity points in the opposite direction of the wormhole rotation, the timelike trajectories can either corotate or contrarotate the wormhole throat.

## V. CONCLUSION AND OUTLOOK

In this paper, we discussed lightlike and timelike geodesics within the simplified Teo wormhole spacetime. We have also shown how to empirically study and detect periodic orbits. To keep the analysis simple, we concentrated on equatorial orbits, but the reader is encouraged to study geodesics that are not restricted to the $(\vartheta = \pi/2)$ hypersurface. Such an exploration could be an interesting exercise for an advanced course in general relativity.

So far, we have investigated only the motion of neutral test particles. Hence, the next step would be to study charged

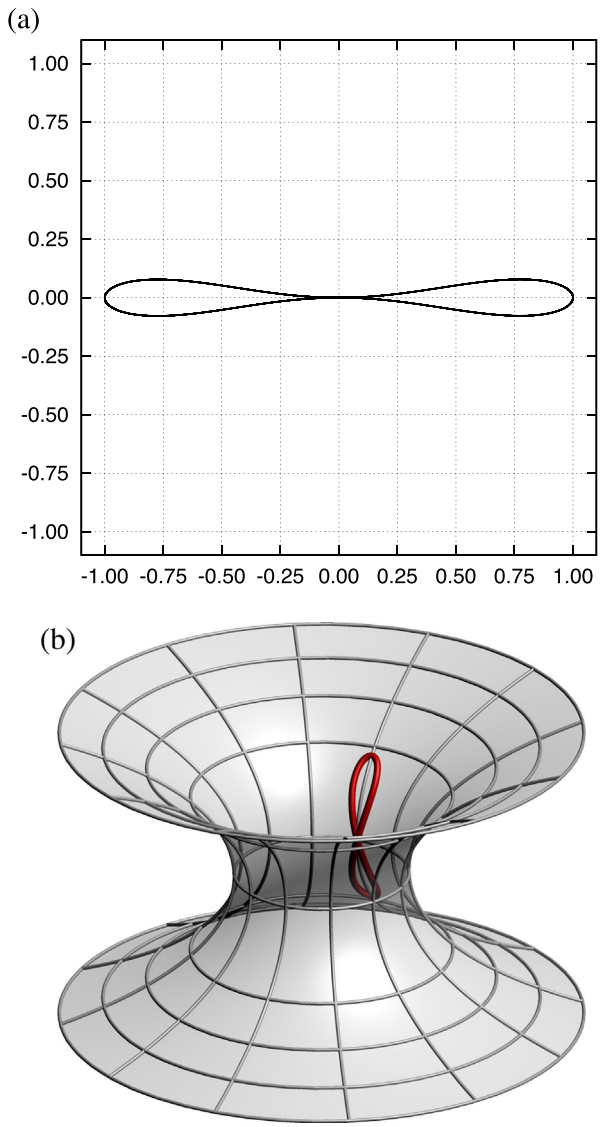


Fig. 8. (a) $xy$-plot and (b) embedding diagram for $\bar{\varphi} = 0$ and $\beta = -0.316205$.

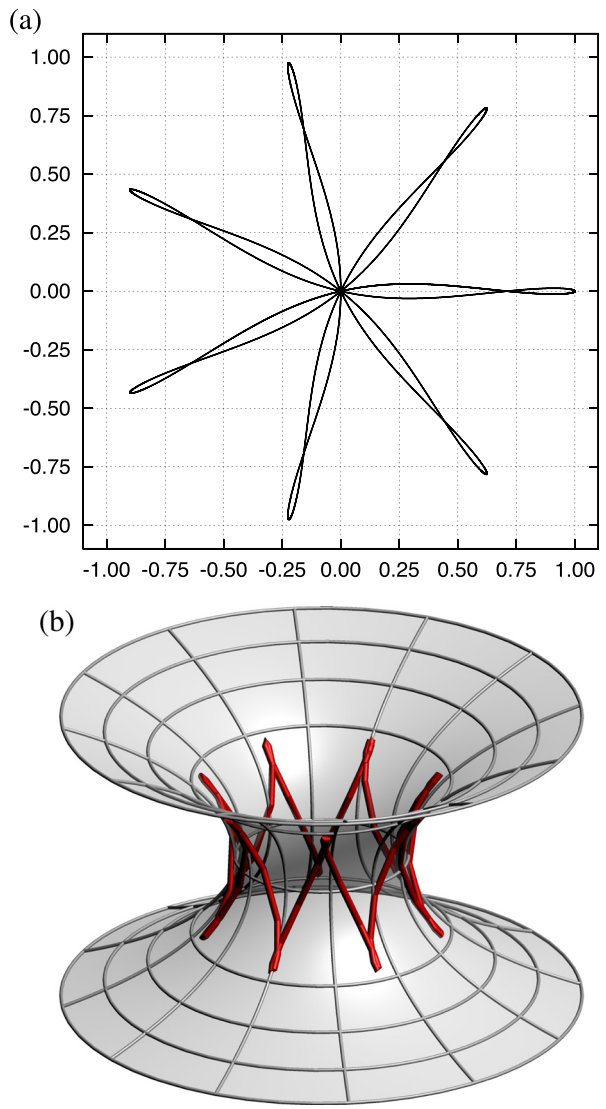


Fig. 9. (a) $xy$-plot and (b) embedding diagram for $\bar{\varphi} = 1/28$ and $\beta = -0.266165$.

particles that might also have some spin and how they move in wormhole spacetimes.

## APPENDIX A: RESTRICTIONS OF THE GRAVITATIONAL POTENTIALS

For educational purposes, we restrict the gravitational potentials in the following way. Please note that this is only a brief outline, a more elucidated discussion can be found in the thesis by Fechtig.[21]

In the limit $r \to \infty$, the Teo metric should tend to the Minkowski metric. Hence,

$$\lim_{r\to\infty} \frac{b(r)}{r} \to 0, \quad \lim_{r\to\infty} N(r,\vartheta) \to 1, \tag{A1a}$$

and

$$\lim_{r\to\infty} \omega(r,\vartheta) \to 0, \quad \lim_{r\to\infty} K(r,\vartheta) \to 1. \tag{A1b}$$

The flare-out condition (FOC), which is responsible for the wormhole throat to be continuous, smooth, and a minimal surface, yields the constraint equation

$$2r(r-b)(2K' + rK'') - (K + rK')(rb' - b) > 0, \tag{A2}$$

where a prime denotes the derivative with respect to $r$.

Motivated by the Kerr spacetime, we make use of the Hamilton-Jacobi formalism and search for a Carter-like constant, which also implies that the equations of motion should be separable. This finally leads to the conditions

$$\lim_{r\to\infty} K(r,\vartheta) = \lim_{r\to\infty} \frac{R(r)}{\Theta(\vartheta)} = \frac{1}{\Theta(\vartheta)} \lim_{r\to\infty} R(r) \to 1, \tag{A3a}$$

or

$$\lim_{r\to\infty} R(r) \to \Theta(\vartheta). \tag{A3b}$$

Thus, $\Theta(\vartheta) = \text{const}$, and neither of the potentials can depend on $\vartheta$. Then, a first ansatz could be

$$b(r) = b_0 \left(\frac{b_0}{r}\right)^m, \tag{A4a}$$

and

$$K(r) = \left[1 + \left(\frac{b(r)}{r}\right)\right], \quad (m,n) \in \mathbb{R} \tag{A4b}$$

which turns the FOC into the algebraic equation

$$(m+1)[2 - n(m+1)] > 0, \quad \text{for} \quad r = b_0. \tag{A5}$$

Because of the asymptotic flatness requirement, the parameter $m > -1$ and Eq. (A5) reduces to $n(m+1) < 2$. For the angular velocity, we make the ansatz

$$\omega(r) = \frac{c}{2b_0} \left(\frac{b_0}{r}\right)^k, \quad k \in \mathbb{R}. \tag{A6}$$

The absence of an ergosphere requires $k \geq 1$. Like Teo, we set $N(r) = K(r)$. Hence, our final choice $m = 1$, $n = 0$, $k = 3$ yields the potentials given in Eq. (2).

## APPENDIX B: STRESS-ENERGY TENSOR

The drawback of any wormhole geometry is the necessity of exotic matter in a non-negligible amount, which prevents even future civilizations from travelling through these shortcuts in spacetime. In order to show that this circumstance is also true for the Teo wormhole spacetime with the chosen potentials, we determine the stress-energy tensor $T_{(i)(j)}$ with respect to the locally non-rotating frame [see Eq. (8)]. By means of Einstein's field equations $G^{(i)(j)} = \kappa T^{(i)(j)}$ with $\kappa = 8\pi G/c^4$, the stress-energy tensor is directly related to the Einstein-Tensor $G^{(i)(j)} = G^{\mu\nu}\theta^{(i)}_{\mu}\theta^{(j)}_{\nu}$. Here, $G_{\mu\nu}$ is the usual coordinate representation of the Einstein tensor, which could be calculated with symbolic math software like Maple (GRTensorII)[22] or Mathematica, and $\theta^{(i)}_{\mu}$ are the dual tetrad vector components following from the relation $\langle \theta^{(i)}, \mathbf{e}_{(j)} \rangle = \delta^{(i)}_{(j)}$ with the Kronecker-$\delta$. As we immediately see from the Einstein tensor

$$G^{(t)(t)} = -\frac{b_0^4\left[16\left(l^2 + b_0^2\right)^2 + 9b_0^2 l^2 \sin^2\vartheta\right]}{16\left(l^2 + b_0^2\right)^4}, \tag{B1a}$$

$$G^{(t)(\varphi)} = \frac{3b_0^4 \sin\vartheta}{4\left(l^2 + b_0^2\right)^3}, \tag{B1b}$$

$$G_{(l)(l)} = -\frac{b_0^4\left[16\left(l^2 + b_0^2\right)^2 - 9b_0^2 l^2 \sin^2\vartheta\right]}{16\left(l^2 + b_0^2\right)^4}, \tag{B1c}$$

$$G^{(\vartheta)(\vartheta)} = \frac{b_0^4\left[16\left(l^2 + b_0^2\right)^2 - 9b_0^2 l^2 \sin^2\vartheta\right]}{16\left(l^2 + b_0^2\right)^4}, \tag{B1d}$$

and

$$G^{(\varphi)(\varphi)} = \frac{b_0^4\left[16\left(l^2 + b_0^2\right)^2 - 27b_0^2 l^2 \sin^2\vartheta\right]}{16\left(l^2 + b_0^2\right)^4}, \tag{B1e}$$

where the $(t)(t)$- and $(l)(l)$-components are always negative, resulting in both a negative energy density and a negative pressure term.

[a]Electronic mail: thomas.mueller@vis.uni-stuttgart.de
[b]Electronic mail: oli.fechtig@gmx.de

[1]M. M. Morris and K. S. Thorne, "Wormholes in spacetime and their use for interstellar travel: A tool for teaching general relativity," Am. J. Phys. **56**, 395–412 (1988).
[2]H. Ellis, "Ether flow through a drainhole: A particle model in general relativity," J. Math. Phys. **14**, 104–118 (1973).
[3]The wormhole metric announced in the paper by Morris and Thorne (Ref. 1) should correctly be called Ellis wormhole.
[4]O. James, E. von Tunzelmann, P. Franklin, and K. S. Thorne, "Visualizing interstellar's wormhole," Am. J. Phys. **83**, 486–499 (2015).
[5]W. Rindler, *Relativity—Special, General and Cosmology* (Oxford U.P., Oxford, 2001).
[6]E. Teo, "Rotating traversable wormholes," Phys. Rev. D **58**, 024014 (1998).
[7]T. Müller, "Exact geometric optics in a Morris-Thorne wormhole spacetime," Phys. Rev. D **77**, 044043 (2008).
[8]J. Levin and G. Perez-Giz, "A periodic table for black hole orbits," Phys. Rev. D **77**, 103005 (2008).
[9]J. Levin and G. Perez-Giz, "Homoclinic orbits around spinning black holes. I. Exact solution for the Kerr separatrix," Phys. Rev. D **79**, 124013 (2009).
[10]R. Fujita and W. Hikida, "Analytical solutions of bound timelike geodesic orbits in Kerr spacetime," Class. Quantum Grav. **26**, 135002 (2009).

[11]Z. Kh. Kurmakaev, "Circular orbits in the Kerr metric," Sov. Astron. **18**, 110–111 (1974).
[12]D. Bini and R. T. Jantzen, "Circular orbits in Kerr spacetime: Equatorial plane embedding diagrams," Class. Quantum Grav. **17**, 1637–1647 (2000).
[13]D. Pugliese, H. Quevedo, and R. Ruffini, "Circular motion of neutral test particles in Reissner-Nordström spacetime," Phys. Rev. D **83**, 024021 (2011).
[14]A. Wünsch, T. Müller, D. Weiskopf, and G. Wunner, "Circular orbits in the extreme Reissner-Nordstrøm dihole metric," Phys. Rev. D **87**, 024007 (2013).
[15]M. Visser, *Lorentzian Wormholes—From Einstein to Hawking* (Springer, New York, 1996).
[16]T. Müller, "GeodesicViewer—A tool for exploring geodesics in the theory of relativity," Comput. Phys. Commun. **181**, 413–419 (2010).
[17]T. Müller and J. Frauendiener, "Studying null- and time-like geodesics in the classroom," Eur. J. Phys. **32**, 747–759 (2011).
[18]T. Müller and F. Grave, "Motion4D—A library for lightrays and timelike geodesics in the theory of relativity," Comput. Phys. Commun. **180**, 2355–2360 (2009).
[19]C. W. Misner, K. S. Thorne, and J. A. Wheeler, *Gravitation* (W. H. Freeman, New York, 1973).
[20]Gnuplot is a portable command-line driven graphing utility, see <http://www.gnuplot.info>.
[21]O. Fechtig, "Physikalische Aspekte und Visualisierung von stationären wurmlöchern," diploma thesis (in German), University of Stuttgart, Stuttgart, Germany, ITP1 (2004); <http://itp1.uni-stuttgart.de/publikationen/abschlussarbeiten/fechtig_diplom_2004.pdf>.
[22]GRTensor II is a computer algebra package that was originally developed for Maple V, see <http://grtensor.phy.queensu.ca>.

**Polarization Apparatus**

This is a "modern" version of the classic Nörrenberg Doubler that was devised in 1858. Light from the mirror strikes the tilted black surface at Brewster's angle and reflects upward into the lens system. At the top is a Nicol (polarizing) prism that is set to let no light through. The example to be examined between the crossed polarizers is placed just under the Nicol prism. The example is in the Greenslade Collection and was priced at 175 marks (about $45) in the 1900 catalogue of Max Kohl of Chemnitz, Germany. (Notes and picture by Thomas B. Greenslade, Jr., Kenyon College)